

# High Contrast Imaging with Gaussian Aperture Pupil Masks

John H. Debes, Jian Ge, Caylin Mendelowitz, and Anne Watson

Pennsylvania State University, 525 Davey Lab, University Park, USA

## ABSTRACT

Gaussian aperture pupil masks (GAPMs) can in theory achieve the contrast requisite for directly imaging an extrasolar planet. We outline the process of fabricating and testing a GAPM for use on the Penn State near-IR Imager and Spectrograph (PIRIS) at the Mt. Wilson 100" telescope. We find that the initial prototype observations are quite successful, achieving a contrast similar to a traditional Lyot coronagraph without blocking any light from a central object and useful for finding faint companions to nearby young solar analogues. In the lab we can reproduce the expected PSF to within an order of magnitude and with new designs achieve  $\sim 5 \times 10^{-5}$  contrast at  $10\lambda/D$ . We find that small inaccuracies in the mask fabrication process and insufficient correction of the atmosphere contribute the most degradation to contrast. Finally we compare the performance of GAPMs and Lyot coronagraphs of similar throughput.

**Keywords:** high contrast imaging, apodization, extrasolar planets, coronagraphy

## 1. INTRODUCTION

The search to directly image an extrasolar planet requires contrast levels of  $\sim 10^{-9}$  a few  $\lambda/D$  from the central star. Scattered light in a telescope and the diffraction pattern of the telescope's aperture limit the contrast possible for direct detection of faint companions. The circular aperture of telescopes creates a sub-optimal diffraction pattern, the so-called Airy Pattern which is azimuthally symmetric. In addition, the intensity in the diffraction pattern of the circular aperture declines as  $\theta^{-3}$ . Currently the best way to diminish the Airy pattern is to use a coronagraph by using the combination of a stop in the focal plane that rejects a majority of the central bright object's light and a Lyot stop in the pupil plane to reject high frequency light.<sup>1-3</sup> Several recent ideas explore the use of alternative "apodized" apertures for high contrast imaging in the optical or near-infrared.<sup>4-6</sup> These designs revisit concepts first experimented with in the field of optics.<sup>7</sup> Other designs, such as the band limited mask, seek to null the light from a central star in much the same way that a nulling interferometer performs.<sup>8</sup>

All of these designs in theory can reach the contrast ratio necessary for imaging a planetary companion, however most of these designs have yet to be tested in the lab or on a real telescope where other concerns arise. The specific advantages of each idea cannot be determined until they are actually built or modeled in such a way as to simulate real engineering problems.

A promising design for a shaped aperture was recently suggested by Ref. 5. In this case the top and bottom edges of the aperture are described by gaussian functions:

$$y_t = aR \left\{ \exp \left[ -(\alpha x/R)^2 \right] - \exp(-\alpha^2) \right\} \quad (1)$$

$$y_b = -bR \left\{ \exp \left[ -(\alpha x/R)^2 \right] - \exp(-\alpha^2) \right\}, \quad (2)$$

where  $x$  goes from  $-R < x < R$ . The Fourier transform of the aperture shape function gives the resulting diffraction pattern in the imaging plane. Since the Fourier transform of a gaussian is another gaussian, the intensity of the diffraction pattern  $I(\epsilon, \eta)$  along one image plane axis decreases exponentially, which we denote the high contrast axis. The ratio  $z = I(\epsilon, \eta)/I(0)$  gives the contrast relative to the peak intensity of the diffraction pattern. The variables  $a, b$ , and  $\alpha$  are all free parameters that can be used to optimize the aperture for depth of contrast, the angle from the central object at which high contrast starts, and the azimuthal area of high contrast.

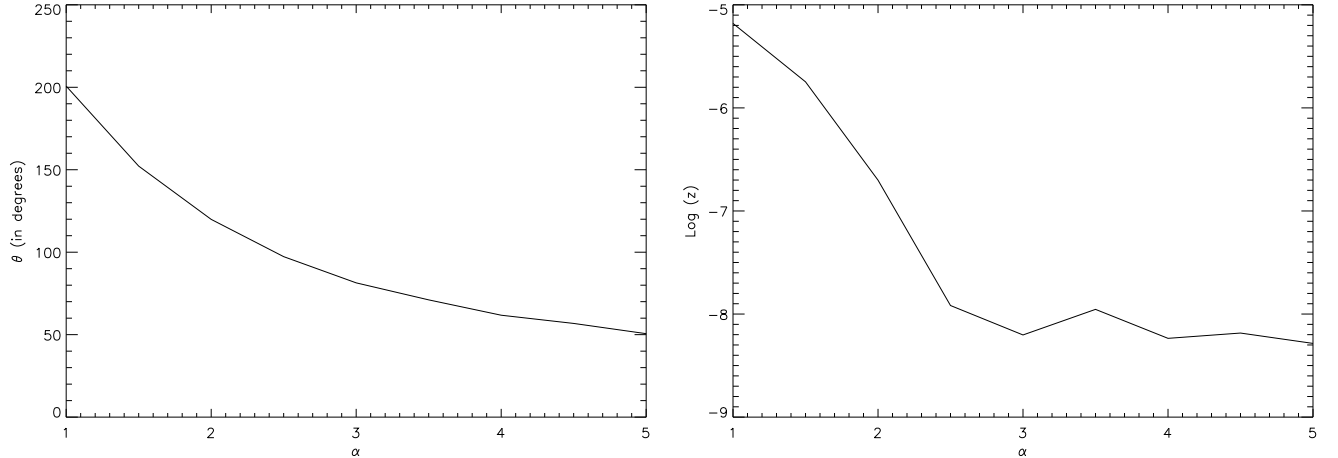


**Figure 1.** (left) The log of normalized contrast vs.  $\alpha$ . As  $\alpha$  increases the contrast ratio decreases sharply, but at the cost of where the contrast begins. (right) The dependence of search angle  $\theta$  with increasing  $\alpha$ . A larger  $\alpha$  restricts the total region of high contrast.

By placing a mask into the pupil plane with a gaussian aperture, one can transform a traditional circular aperture telescope into one with a diffraction pattern better suited for high contrast imaging. Using a mask represents a quick, efficient, and cheap way to test this emerging imaging method to determine its advantages and tradeoffs and compare them to the performance of other existing techniques.

We have endeavored to begin answering the question of which design ultimately will be useful in the search for extrasolar planets, or which will be most useful for other areas of astronomy where less stringent tolerances are present. To that end we have designed, fabricated, and tested several GAPM designs for use with the Penn State near-IR Imager and Spectrograph (PIRIS).<sup>6</sup> In Section 2 we explore what the best design for a telescope would be. In Section 3 we briefly discuss the process of fabrication of the GAPMs, while in 4 we discuss the various tests we performed in the lab and on the ground at the Mt. Wilson 100" telescope. In Section 5 We compare the contrast of GAPMs with comparable Lyot coronagraphs Finally in section 6 we discuss what role GAPMs have for future high contrast imaging.

## 2. DESIGNING A GAPM FOR CURRENT TELESCOPES

The idealized design of a single gaussian aperture in practice cannot be used on current telescopes due to their circular secondary obstructions and the presence of the support structure. These two additions serve to modify the resulting diffraction pattern and destroy the advantages of the single aperture. Therefore, a new design that avoids or minimizes their effect is necessary to retain high contrast. In order to design a GAPM for use on the Mt. Wilson 100" telescope, we performed several numerical simulations to determine the design that had the best theoretical performance. In addition we quantify how the presence of a secondary mirror and support structure degrade contrast.

### 2.1. Modeling Different Apertures

In order to test the performance of different designs, we have created several IDL programs to model the resulting diffraction patterns or point spread functions (PSFs) from different apertures. In its simplest form, the models determine the Fraunhofer diffraction of light through an aperture. The diffraction is calculated by performing a Fast Fourier Transform (FFT) algorithm on an incoming wavefront, represented by a complex 2D array. Taking the real part of the resultant amplitude image and squaring it gives the intensity.

The complete model calculates the diffraction of a light wave's amplitude first passing through the circular aperture of a telescope with a secondary mirror and support structure. An input wavefront array with the shape

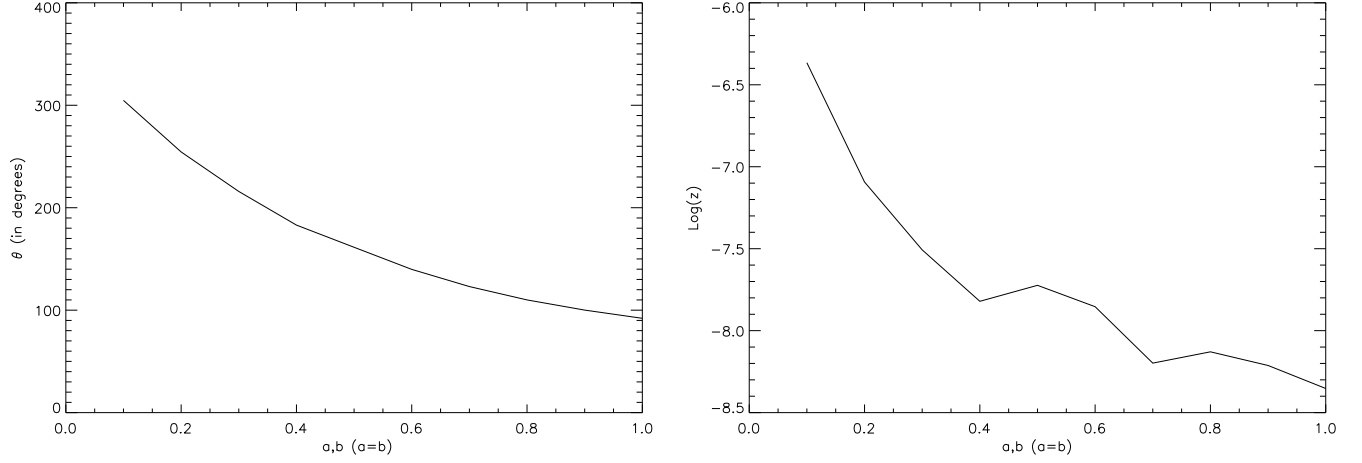


**Figure 2.** Same as for Figure 1 but for varying  $a, b$  where  $a = b$ . Decreasing  $a$  or  $b$  can increase search angle but decrease throughput and degrade contrast.

of the pupil undergoes an FFT to give a PSF of the telescope. After calculating the PSF of the aperture, an ideal test image can be convolved with the PSF. This allows an independent calculation of the contrast possible for a given design by creating an image of a central object and a companion of a given flux ratio. A crucial issue for any design is its ability to not only achieve a high contrast, but do so in a way that does not seriously degrade the intrinsic resolution of the companion PSF. An example would be an overly ambitious undersizing of a Lyot stop. While in theory this can provide very high contrast, the smaller aperture size essentially spreads out the light of any faint companion and drastically increases the integration time, making it harder to detect.

After convolution with the image, the array is then multiplied with the transmission of a focal plane mask, which can either be empty or have some coronagraphic spot present. Next the array undergoes an inverse FFT which results in the intensity pattern at the pupil plane. A pupil mask transmission function is then multiplied with the array and undergoes one final FFT to create the image on the detector. In order to have sufficient resolution and keep aliasing affects to a level of  $<10^{-8}$ , most simulations were performed with  $2048 \times 2048$  element arrays where the pupil was undersized by a factor of two. The model does not include wavefront errors, residual scattered light, or atmospheric turbulence. A single wavelength PSF is generated.

## 2.2. Testing Initial Designs

Studying the effect of varying  $a, b$ , and  $\alpha$  is instructive in understanding the best values to use for a given situation. For the initial test of a prototype design, a balance of search area and depth of contrast was most useful. Figure 1 shows the effect of varying  $\alpha$  on  $z$  along the axis of highest contrast. Around  $\alpha=2.7$  one can see that the contrast doesn't improve due to the resolution of the simulations. To determine  $z$  we took ten points centered at  $\sim 10 - 20\lambda/D$  depending on where the region of high contrast occurred and averaged their value of  $z$ . In general, increasing  $\alpha$  will decrease  $z$ , but at the cost of the region of high contrast starting at a larger  $\lambda/D$ .

Another important factor is determining the azimuthal coverage of the region of high contrast. we measured this quantity,  $\theta$  by calculating the region that had  $z < 10 z_{hc}$  where  $z_{hc}$  is the contrast ratio along the high contrast axis at the. Figure 1 shows the variation of  $\theta$  with  $\alpha$ . As  $\alpha$  increases,  $\theta$  decreases.

Varying  $a$  and  $b$  can also affect azimuthal coverage and contrast. In general decreasing  $a$  and  $b$  has the affect of increasing azimuthal coverage with the tradeoff of a reduced contrast. As an example we have plotted both  $\theta$  vs.  $a, b$  and  $\log z$  vs.  $a, b$  (see Figure 2). Decreasing  $a$  and  $b$  also reduces throughput.

As mentioned before, a single open aperture is degraded severely by the addition of a secondary and support structure. It is then necessary to determine a design that avoids the problems associated with these structures.

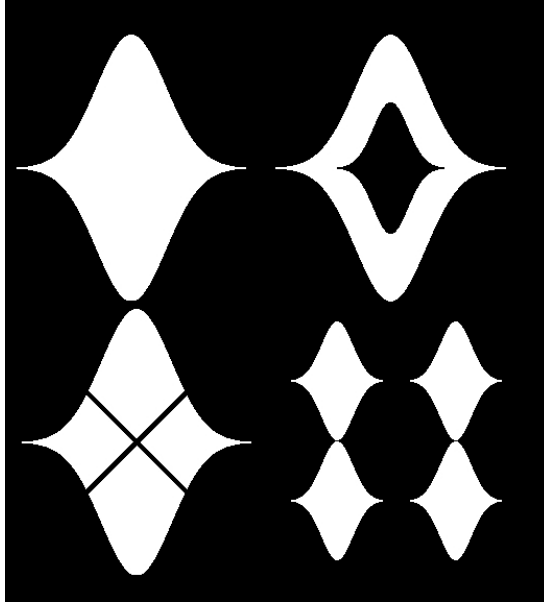


**Figure 3.** The designs tested in our simulations. The upper left is the single aperture design, upper right single aperture with secondary, lower left single aperture with support structure, and lower right multiple aperture design.

Two types of designs are immediately apparent, either mitigating the effect of the secondary mirror or avoiding the secondary and support structures altogether.

We created four designs to test with our simulations in order to gauge the degradation in contrast from the ideal case and to determine what configuration was the best. The four designs are shown in figure 3. The first is an ideal case, a single gaussian aperture with  $\alpha=2.7$  and  $a = b = 1$ . The second design is a single gaussian aperture with a smaller gaussian stop that blocks the circular secondary completely, but with no support structure. A third design has only a support structure, in order to disentangle the level of degradation of the two designs. The orientation of the support structure is crucial, since the spider arms can completely ruin the high contrast axis if positioned perpendicular to the mask's horizontal axis. The best design requires that the support structure is rotated  $45^\circ$  with respect to the horizontal axis. When that is done the resulting diffraction spikes are arrayed in the brighter regions of the pattern. The final design has four gaussian apertures that are equal to half the total width of the single aperture and avoid any other structure.

Figure 4 shows the results of two of our simulations, the multiple opening mask and the mask with a secondary and demonstrates the basic diffraction pattern of a gaussian aperture. The peak is surrounded by two different regions, a dark high contrast region around the horizontal axis and a brighter low contrast region in an hourglass shape centered vertically from the peak. The gaussian aperture effectively redistributes the light from the central object, leaving a region with little light.

Compared to the single opening mask, the mask with a secondary has a much wider bright central region and a slightly smaller search area. The four opening approach has an overall similarity to the single opening mask, but has an elevated background and less resolution due to the smaller opening. In order to quantify the contrast, each design's ratio of intensity to the peak was averaged between  $10\lambda/D$  and  $20\lambda/D$  along the high contrast axis. This was performed over a large range of simulation array sizes to determine the best array size.

Figure 6 shows the full results and demonstrates the problems of adding a gaussian secondary and support structures. The secondary, while an improvement over a circular shape, still degrades contrast close to the central object. At larger distances the secondary has a contrast similar to the single opening design. The support structure for all the array sizes was chosen to be .2% of the primary size (the approximate ratio at the Mt. Wilson telescope). We find that this degrades contrast by  $\sim 2$ -3 orders of magnitude. The multi-aperture

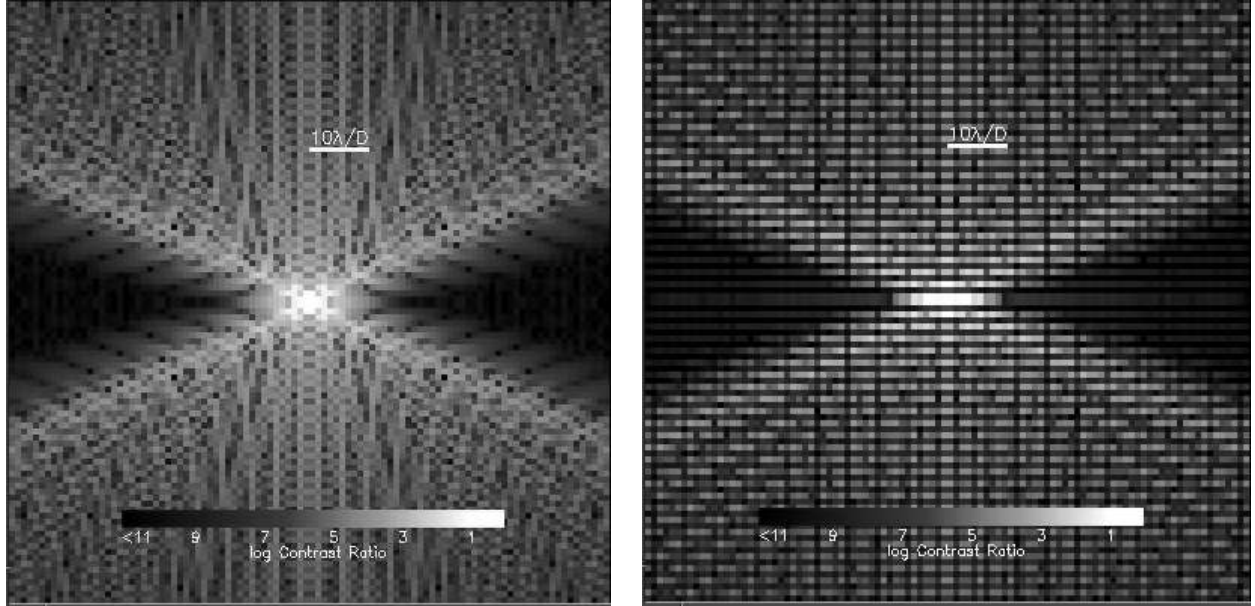


**Figure 4.** The resulting diffraction patterns for the single aperture with secondary design (left) and the multiple aperture design (right). The images are logarithmically scaled.

design has slightly degraded contrast, and a major trade off is a twofold decrease in resolution due to the halving of the aperture width. Even with this degradation in resolution, it performs better than the gaussian secondary and support structure combined.

Our final design used the multi-aperture approach. We chose  $\alpha=2.7$ ,  $a = .23$  and  $b = .33$  to give a  $z=10^{-76}$  contrast and  $180^\circ$  azimuthal coverage. Figure 5 shows the design and the resulting diffraction pattern. We arrayed 12 apertures in a pattern symmetric about the center for added throughput, coming to  $\sim 25\%$  compared to a completely open pupil. The azimuthal coverage is  $\sim 3$  times better at a  $z=10^{-6}$  than the single opening design, and suffers two orders of magnitude degradation in contrast.

### 3. FABRICATING A GAPM

Once a design was chosen the masks were fabricated. For the initial observing run at Mt. Wilson, we chose to have the masks made by Photo-Chemical Machining (PCM). This technique has been used to produce masks to block thermal radiation from telescope structures for near-IR observing and for creating Lyot stops.

The process of PCM, also called Photo-Etching or Photo-Chemical Milling, involves using a thin metal sheet that is coated with a light sensitive polymer. Then a UV photo imaging tool is used to imprint the desired design on the sheet. It is then developed much like film and chemically etched by an aqueous solution of ferric chloride ( $\text{FeCl}_3$ ).

Several masks are present in the PIRIS camera mainly for the traditional lyot coronagraphic modes. They were fabricated by Newcut, Inc. (Newark, NJ). For the GAPMs we submitted CAD designs based on the simulations performed to Newcut and they fabricated the masks. A sheet of 25-50 masks with a diameter of  $\sim 4$  mm were fabricated at very low cost within a few weeks. When they were delivered they were photographed on an optical telescope with 5x and 50x magnification.

This technique can provide the basic shape we need, but has difficulty preserving the exact shape of the design in the smallest regions. The edges of the gaussians on the mask were truncated well before they mathematically would be. Variations on the order of  $10\mu\text{m}$  are also observed in the masks. Both of these imperfections can degrade contrast, which is discussed further in Section 4. These imperfections are likely caused by the photo

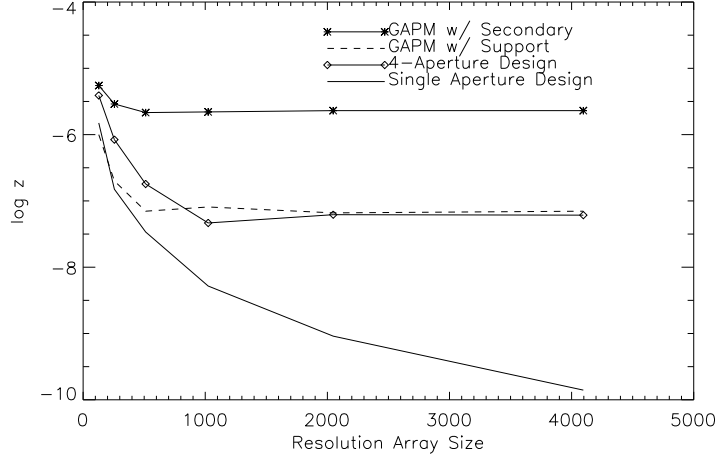


**Figure 5.** Contrast as a function of simulation array size for different types of designs.

printing as well as the chemical etching. for instance, the corner truncation and width variation can be caused by underexposure of the light sensitive polymer. The rugged edge can be caused by non-uniform chemical etching. Since the etching is isotropic, local changes in the physical and chemical conditions of the etchant cause irregularities.

#### 4. TESTING THE PROTOTYPE

We placed the fabricated pupil mask on the Penn State Near-IR Imager and Spectrograph (PIRIS) and ran tests both in the lab and on the 100" Mt. Wilson telescope. We used the prototype as part of a survey for faint companions around nearby solar type stars.<sup>9,10</sup> The stars  $\epsilon$  Eridani (GJ 144 = HD 22049 = HR 1084,  $V=3.72$ ,  $d=3.2$  pc) and  $\mu$  Her A (GJ 695A = HD 161797 = HR 6623,  $V=3.41$ ,  $d=8.4$  pc) were observed with the GAPM. The star  $\epsilon$  Eridani was observed with seven 4s integrations in the K band, while  $\mu$  Her A was observed with one 3s and one 10s integration in the H band. Both objects were also observed in normal imaging modes. The plate scale and orientation for PIRIS was determined by measuring the positions of several stars in the Orion Nebula and comparing them to 2MASS data. We find that the plate scale of PIRIS is  $.082'' \pm .001'' \text{ pixel}^{-1}$ .

The GAPM was aligned  $23^\circ$  clockwise from North to line up with the support structure of the telescope. Therefore, the axis of greatest contrast would be oriented perpendicular to the alignment of the mask or along a line running from the NW to the SE in an image.

For our coronagraphic modes we used a stop in the focal plane that has a gaussian transmission function<sup>11</sup> with a fwhm of  $\sim 1.1''$  in an image. A Lyot stop was placed in the pupil plane whose dimensions were chosen for an optimal combination of throughput and contrast (See Ref 10).

In order to test the level of contrast achieved by the gaussian mask in comparison to other modes of PIRIS, coronagraphic and adaptive optics observations were taken of the star+faint companion system Gl 105.<sup>12,13</sup> Figure 7 shows the differences in the three modes. The observations were azimuthally averaged in high contrast areas. For Gl 105, we azimuthally averaged the PSF with the exception of  $35^\circ$  on either side of the faint companion. The resulting profiles were then normalized to peak flux. Further scaling had to be performed for the coronagraphic and gaussian pupil mask profiles. In these two cases the peak flux could not be determined due to the coronagraphic mask for Gl 105 and due to saturation for  $\epsilon$  Eridani. In the case of Gl 105 this problem was circumvented by the presence of the companion which was used to properly scale the flux. The error in the curve for the coronagraph is due mostly to uncertainties in the positions and flux ratio of the companion and the central star, but should be no larger than on the order of 10%. In the case of  $\epsilon$  Eridani we took unsaturated images of a dimmer standard star and normalized the azimuthally averaged PSF at  $.82''$ . The profile of the GAPM is a composite of those two sets of observations. The error in this normalization is dominated by

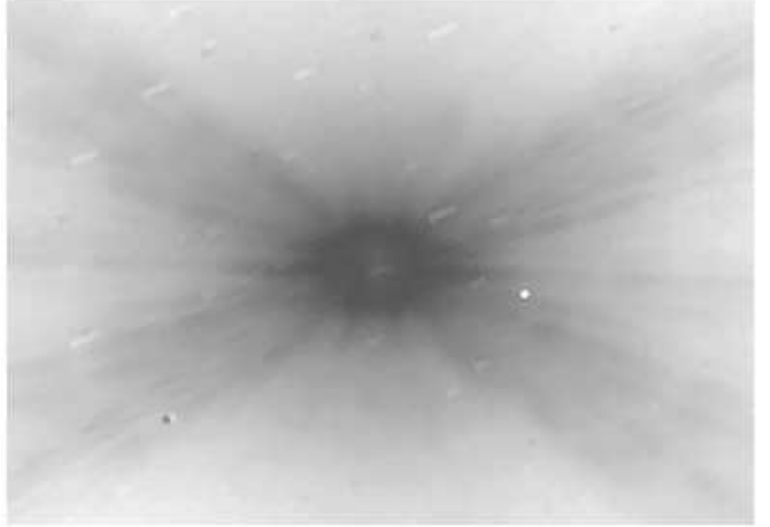
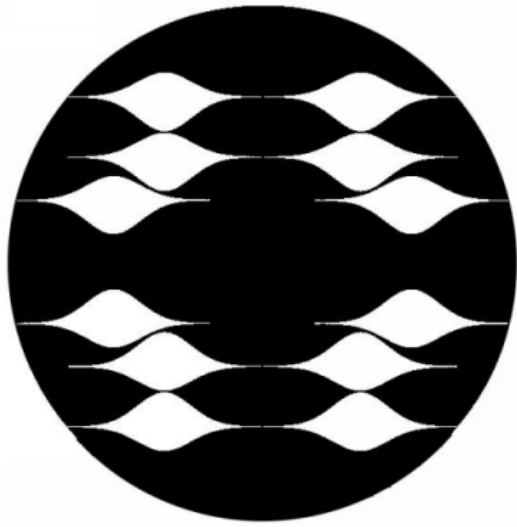


**Figure 6.** Picture of the final design and of the resulting diffraction pattern at Mt. Wilson telescope.

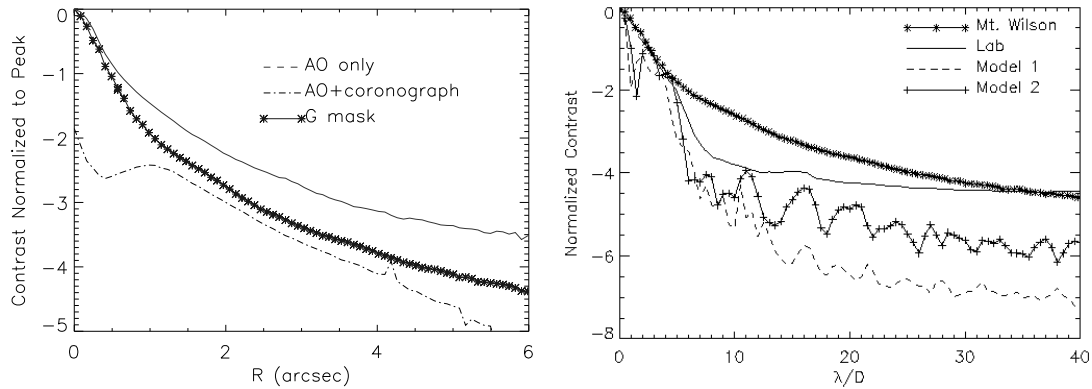


**Figure 7.** (left) Azimuthally averaged PSF profiles for three different modes observed with on the Mt. Wilson telescope. (right) Azimuthally averaged PSF profiles for the GAPM multiaperture design tested at Mt. Wilson, along with results of a lab test and two different models.

variations in the PSF and to estimate the effects of this we varied the point at which we normalized the two profiles. We found that at most the error introduced is of the order 25%.

As can be seen in Figure 7, the GAPM performs better than AO alone and is  $\sim 2$  times worse than a traditional coronagraph  $> 1''$ . This is without any attempt to block the light of the central star.

Lab testing was also performed in the J band. The setup involved taking an incandescent lamp and simulating a point source to sample the PSF generated by the different masks. An optical fiber took light from an incandescent lamp where it passed through a micro objective and a pinhole. The light then was collimated by a collimator achromat. After the collimator it was focused onto the slit wheel aperture by an image achromat. The image achromat also forms an exit pupil, 1.9 m away from the focal plane, mimicking the Mt. Wilson 100inch exit pupil. On the slit wheel we placed our focal plane coronagraphic masks. The light then travels through the camera optics of PIRIS where it is read by the  $256 \times 256$  PICNIC array.

Figure 7 shows an azimuthally averaged comparison between the data taken at Mt. Wilson, lab tests, and two theoretical simulations as a function of  $\lambda/D$ . One simulation, called model 1, represents a completely ideal situation where the mask is perfectly created and no wavefront errors exist. The second simulation, model 2,

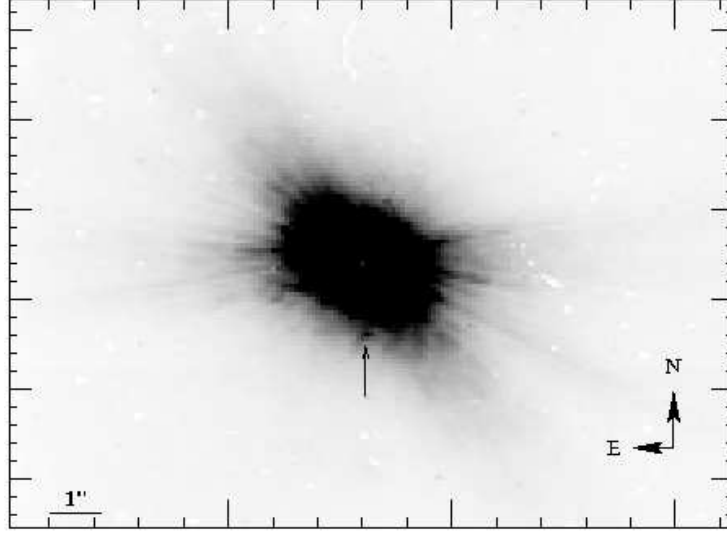


**Figure 8.** Raw Image of Mu Her A.

takes the observed shape of the masks under magnification as the apertures and neglects other errors. All of the data and simulations were averaged over the same angle. One can see that the theoretical simulation of the observed shape matches the lab data quite well, off by less than an order of magnitude close to the center. The observed shape errors also degrade the contrast achievable by the idealized design. Finally the effect of the atmosphere is present in the Mt. Wilson data, which further degrades the contrast from what is possible.

From the azimuthally averaged profiles, limits to the type of companions we could have detected around  $\epsilon$  Eridani can be estimated. Beyond  $4''$  ( $\sim 13$  AU), any companion with  $\Delta m_K < 9.3$  mag would have been detected, and at  $8''$  ( $\sim 26$  AU) any companion  $< 11.8$  mag would have been detected. These translate to  $M_K$  of 13.6 and 16.1 respectively. We looked at the models of Ref. 14 and Ref. 15 to determine the range of possible companion masses that we could have detected based on .7 Gyr and  $M_K=13.6$  and 16.1, corresponding to  $38 \pm 8 M_J$  and  $20 \pm 5 M_J$ . We derived these estimates by taking a value intermediate to the two models, while the error represents their spread. These results are reported in more detail in Ref. 10.

A faint companion around  $\mu$  Her A was detected with high S/N in both GAPM and AO images. A raw image of This companion was previously  $\mu$  Her A and its companion is shown in Figure 8 detected in R and I band AO images at Mt. Wilson, and used to explain a radial velocity acceleration corresponding to a  $\sim 30$  yr orbit.<sup>16–18</sup>

Our observations confirm the dimmer object to be a proper motion companion and thus physically bound to the brighter star.<sup>10</sup> H and K adaptive optics images of  $\mu$  Her A were also performed. Unfortunately, standard star measurements with the GAPM could not be performed, but we took H and K photometry with the normal imaging mode of PIRIS. We find that for the companion  $m_H=8.5 \pm .1$  and  $m_K=7.9 \pm .1$ , which corresponds to  $M_H=8.9$  and  $M_K=8.3$ . We used the models of Ref. 19, 20 to conclude that its mass should be  $\sim .13 M_\odot$ . For a more detailed description of our results refer to Ref. 10.

## 5. EQUAL THROUGHPUT COMPARISONS

A fairer comparison between a Lyot coronagraph and the GAPM is to have equal throughput designs and compare their contrast levels. As part of lab experiments that we are performing we compared two new GAPM designs with a Lyot coronagraph that had a comparable throughput. Two types of designs were tested, idealized apertures with no secondary structure and realistic masks that will be used for future observing. Figure 9 shows the four types of masks used, a single gaussian opening accompanied by an ideal Lyot coronagraph undersized by the prescription given in Ref. 3 to give 20% throughput, the same as the GAPM. The multi-aperture GAPM



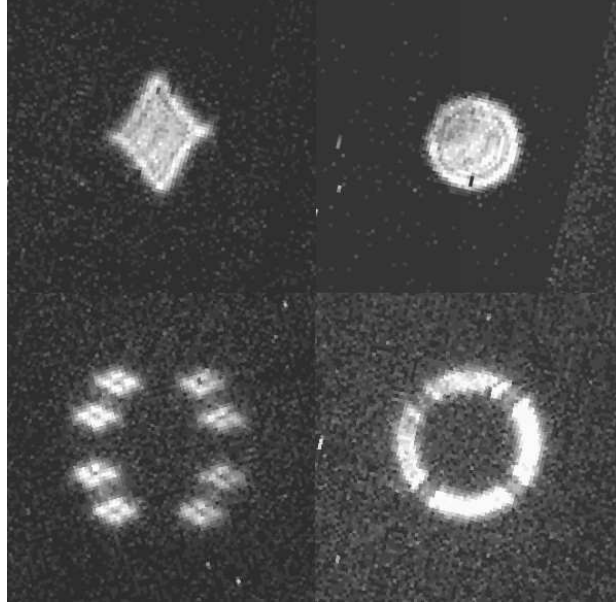


**Figure 9.** Images of the different pupils used for the equal throughput comparisons.

has  $\sim 30\%$  throughput as well as the corresponding Lyot stop. Unsaturated images GAPMs were taken to predict the flux for the longer, saturated images. This predicted flux was used to estimate the peak flux for the longer exposures taken. The critical fact of these experiments is to get enough counts to make sure that the PSF dominates the read noise. We took exposures that had on the order of  $10^7$  counts. We found that this was insufficient to get high S/N on the fainter portions of the PSF and we estimate that beyond  $1\text{-}2''$  the read noise begins to dominate. Longer integrations are planned.

For the coronagraphic modes we used a gaussian transmission focal plane mask with a FWHM of  $500\mu m$ . In the J band this corresponded to a mask with a FWHM of  $\sim 11\lambda/D$ . Short exposures were taken without the mask for estimating the peak flux of an unblocked point source for a given exposure time. The mask was then carefully aligned to within 1 pixel to block the point source.

Figure 10 shows the results of these lab tests, which represents the best performance of our GAPMs and coronagraphic modes. At  $> 10\lambda/D$  the GAPMs perform at  $z = 3 \times 10^{-5}$  for the idealized version and  $z = 6 \times 10^{-5}$  for the multi-aperture design. The coronagraphs perform better, both achieving less than  $10^{-5}$  contrast.

## 6. CONCLUSIONS

We have performed several simulations, lab tests, and telescope observations with GAPMs and Lyot coronagraphs in order to better understand the interplay between theory and the reality of observations. GAPMs alone provide an improvement over a simple circular aperture for quick high contrast imaging. They are very sensitive to an accurate reproduction of shape and thus need accuracies that may be as restrictive as sub-micron precision. This is possible with new nanofabrication techniques that have been perfected at the Penn State Nanofabrication facility, where future masks may be produced. Precisely fabricating these masks can potentially improve performance to the ideal limit for a mask provided it is above the scattered light limit of the telescope, bringing it in line with Lyot coronagraphs of comparable throughput. Demonstration of these masks in conjunction with an active optics system could present a workable example of a quick way to survey for faint companions without needing to incur the overhead cost of precise alignment behind a mask. GAPM performance on the ground will ultimately be limited by the ability of adaptive optics systems to suppress atmospheric turbulence.

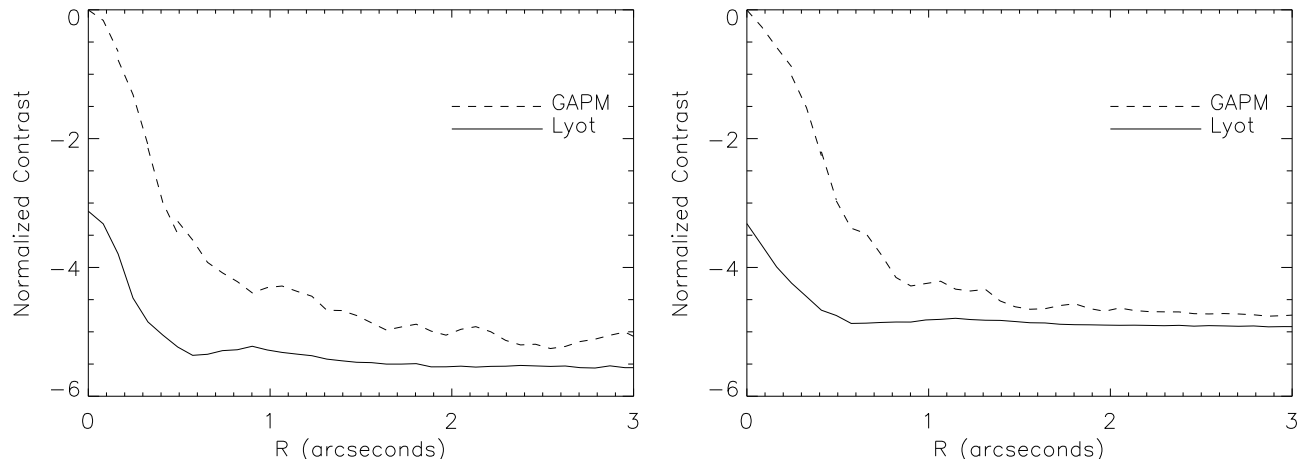


**Figure 10.** Equal throughput comparisons of GAPMs and a Lyot coronagraphs. (left) Azimuthal average of single aperture and idealized Lyot. (right) Azimuthal average of multi-aperture and realistic Lyot.

## ACKNOWLEDGMENTS

The authors would like to acknowledge D. McCarthy for loaning part of the optics for PIRIS, R. Brown (Colorado) for the PICNIC array, C. Ftaclas for coronagraphic masks, and A. Kutyrev for filters. Several important discussions with D. Spergel, M. Kuchner, W. Traub, C. Burrows, and R. Brown (STScI) were crucial in our understanding of gaussian apertures, band limited masks, and HST image performance. We would also like to thank the invaluable help of the the Mt. Wilson staff and L. Engel for design help with the GAPM.

J.D acknowledges funding by a NASA GSRP fellowship under grant NGT5-119. This work was supported by NASA with grants NAG5-10617, NAG5-11427 as well as the Penn State Eberly College of Science.

## REFERENCES

1. B. Lyot, “The study of the solar corona and prominences without eclipses (George Darwin Lecture, 1939),” *MNRAS* **99**, pp. 580–+, June 1939.
2. F. Malbet, “High angular resolution coronagraphy for adaptive optics,” *A & AS* **115**, pp. 161–+, Jan. 1996.
3. A. Sivaramakrishnan, C. D. Koresko, R. B. Makidon, T. Berkefeld, and M. J. Kuchner, “Ground-based Coronagraphy with High-order Adaptive Optics,” *ApJ* **552**, pp. 397–408, May 2001.
4. P. Nisenson and C. Papaliolios, “Detection of Earth-like Planets Using Apodized Telescopes,” *ApJL* **548**, pp. L201–LL205, Feb. 2001.
5. D. N. Spergel, “A gaussian shaped pupil for detecting extrasolar planets,” *astro-ph/0101142*, 2001.
6. J. Ge (*in preparation*), 2002.
7. P. Jacquinot and B. Roizen-Dossier, “Apodisation,” *Progress in Optics* **3**, pp. 31–182, 1964.
8. M. J. Kuchner and W. A. Traub, “A Coronagraph with a Band-limited Mask for Finding Terrestrial Planets,” *ApJ* **570**, pp. 900–908, May 2002.
9. A. Chakraborty, J. Ge, and J. H. Debes, “The Nature of Faint Companions to G-Type Stars from Adaptive Optics,” *AJ* **124**, pp. 1127–1131, Aug. 2002.
10. J. H. Debes, J. Ge, and A. Chakraborty, “First High-Contrast Imaging Using a Gaussian Aperture Pupil Mask,” *ApJL* **572**, pp. L165–LL168, June 2002.
11. T. Nakajima, “Planet detectability by an adaptive optics stellar coronagraph,” *ApJ* **425**, pp. 348–357, Apr. 1994.
12. D. A. Golimowski, W. G. Fastie, D. J. Schroeder, and A. Uomoto, “Hubble Space Telescope Observations of the Very Low Mass Companion to Gliese 105A,” *ApJL* **452**, pp. L125–+, Oct. 1995.

13. D. A. Golimowski, T. J. Henry, J. E. Krist, D. J. Schroeder, G. W. Marcy, D. A. Fischer, and R. P. Butler, "The Very Low Mass Component of the Gliese 105 System," *AJ* **120**, pp. 2082–2088, Oct. 2000.
14. A. Burrows, M. Marley, W. B. Hubbard, J. I. Lunine, T. Guillot, D. Saumon, R. Freedman, D. Sudarsky, and C. Sharp, "A Nongray Theory of Extrasolar Giant Planets and Brown Dwarfs," *ApJ* **491**, pp. 856–+, Dec. 1997.
15. G. Chabrier, I. Baraffe, F. Allard, and P. Hauschildt, "Evolutionary Models for Very Low-Mass Stars and Brown Dwarfs with Dusty Atmospheres," *ApJ* **542**, pp. 464–472, Oct. 2000.
16. N. H. Turner, T. A. t. Brummelaar, H. A. McAlister, B. D. Mason, W. I. Hartkopf, and L. C. Roberts, "Search for Faint Companions to Nearby Solar-like Stars using the Adaptive Optics System at Mount Wilson Observatory," *AJ* **121**, pp. 3254–3258, June 2001.
17. A. Cumming, G. W. Marcy, and R. P. Butler, "The Lick Planet Search: Detectability and Mass Thresholds," *ApJ* **526**, pp. 890–915, Dec. 1999.
18. W. D. Cochran and A. P. Hatzes, "A high-precision radial-velocity survey for other planetary systems," *Ap & SS* **212**, pp. 281–291, Feb. 1994.
19. I. Baraffe, G. Chabrier, F. Allard, and P. H. Hauschildt, "Evolutionary models for solar metallicity low-mass stars: mass-magnitude relationships and color-magnitude diagrams," *A & A* **337**, pp. 403–412, Sept. 1998.
20. I. Baraffe, G. Chabrier, F. Allard, and P. H. Hauschildt, "Evolutionary models for low-mass stars and brown dwarfs: Uncertainties and limits at very young ages," *A & A* **382**, pp. 563–572, Feb. 2002.